of the parallel and perpendicular scattering components (an inelastic spectrometer employing polarized neutrons may also be used for this purpose). If the assumption is made that at low temperatures, when the spin moment is nearly fully aligned, the spin scattering is confined to the perpendicular component, an estimate can be made of the orbital scattering. In practice this is only an upper limit because of the possibly incomplete magnetization of the sample. However, the magnitude observed of about 0.2 eV^{-1} $atom^{-1}$ at energies below 0.04 eV has the predicted order of magnitude.

---

*Visiting scientist from Atomic Energy Research Establishment, Harwell, Berkshire, England.

[1]R. J. Elliott, Proc. Roy. Soc. (London) A235, 289 (1956).

[2]J. E. Hebborn and N. H. March, Advan. Phys. 19, 175 (1970).

[3]E. D. Thompson, Phys. Rev. Letters 19, 635 (1967); H. A. Mook, R. M. Nicklow, E. D. Thompson, and M. K. Wilkinson, J. Appl. Phys. 40, 1450 (1969); F. M. Mueller and J. W. Garland, Bull. Am. Phys. Soc. 13, 58 (1968).

[4]R. D. Lowde and C. G. Windsor, Advan. Phys. 19, 813 (1970).

[5]O. Halpern and M. H. Johnson, Phys. Rev. 55, 898 (1939).

[6]R. Peierls, Z. Physik 80, 763 (1933); J. E. Hebborn and E. H. Sondheimer, J. Phys. Chem. Solids 13, 105 (1960); H. Fukuyama and R. Kubo, J. Phys. Soc. Japan 27, 604 (1969).

[7]M. Shimizu and Y. Takahashi, Phys. Letters 32A, 164 (1970).

[8]J. E. Hebborn and N. H. March, Phys. Letters 29A, 432 (1969).

[9]N. Szabo, Diploma thesis (ETH Zürich, 1967) (unpublished).

[10]T. Schneider, Solid State Commun. 8, 279 (1970).

[11]S. W. Lovesey and C. G. Windsor, J. Phys. Radium 32, 573 (1970).

[12]L. Van Hove, Phys. Rev. 95, 1374 (1954).

[13]See, for example, R. Peierls, *Quantum Theory of Solids* (Oxford U. P., Oxford, England, 1955), Sec. 4.2.

[14]D. F. Johnston, Proc. Phys. Soc. (London) 88, 37 (1966).

[15]A. R. Edmonds, *Angular Momentum in Quantum Mechanics* (Princeton U. P., Princeton, N. J., 1960), Sec. 2.5.

[16]R. Watson and A. Freeman, Acta Cryst. 14, 35 (1961).

[17]H. A. Mook, Phys. Rev. 148, 500 (1966).

PHYSICAL REVIEW B VOLUME 4, NUMBER 9 1 NOVEMBER 1971

Exciton Bands in Antiferromagnetic Cr_2O_3†

R. M. Macfarlane

IBM Research Laboratory, San Jose, California 95114

and

J. W. Allen

Lincoln Laboratory, Massachusetts Institute of Technology, Lexington, Massachusetts 02173

(Received 17 May 1971)

We have calculated the energy dispersion of the lowest eight ^2E Frenkel exciton branches in the four-sublattice antiferromagnet Cr_2O_3. This is the first such calculation for a magnetic insulator. The symmetry properties and $\vec{k}$ dependence of the interion exchange and Coulomb interactions which give rise to dispersion and Davydov splittings are presented in detail. Pairwise matrix elements of the interion Hamiltonian are treated as phenomenological parameters, and in most cases were determined from the $\vec{k}=0$ energies analyzed in an earlier paper. Dispersion curves for five directions in the rhombohedral Brillouin zone, and the exciton density of states, are given. Confirmation of the main features of the calculated exciton bands is provided by a measurement of the exciton-magnon absorption band shape. In the presence of a number of simplifying assumptions, this band shape is given by the joint exciton-magnon density of states. Good agreement between the calculated and observed band shape is obtained.

I. INTRODUCTION

Because of translational symmetry, the optical excitations within the localized electrons of magnetic insulators (usually $d \rightarrow d$ or $f \rightarrow f$ transitions) can properly be described as Frenkel excitons.[1] Coulomb and exchange interactions between the magnetic ions provide the mechanisms for the characteristic exciton properties, viz., Davydov splittings and dispersion. It is of considerable importance to establish the existence of these effects because they provide important insights into the

interion couplings. These couplings are of central importance to magnetic ordering in insulators.

The possibility that fine structure in the optical spectra of magnetic insulators is due to the excitonic nature of the excited states seems first to have been investigated experimentally by Eremenko and Belyaeva[2] in MnF_2. However, they did not find evidence for it. Davydov splittings were subsequently observed in the optical spectra of Cr_2O_3[3,4] and $YCrO_3$,[5,6] and negative exciton dispersion has been invoked[7] to explain the properties of an exciton-magnon absorption and bound state in MnF_2. However, no detailed treatment of exciton dispersion in magnetic insulators has yet been given.

We propose here a model for the interion (exchange) couplings in Cr_2O_3 which give rise to appreciable (~ 100 cm^{-1}) dispersion of the ^2E excitons. This work is an extension of our earlier analysis of the $\vec{k} \simeq 0$ excitons (hereafter referred to as AMW[4]). For several reasons, the ^2E excitons in Cr_2O_3 provide one of the best examples in magnetic insulators for a study of exciton effects. The Cr^{3+} ion states involved have a relatively simple structure, being predominantly $t_2^3\,{}^4A_2$ and $t_2^3\,{}^2E$. The spectrum of the dilute paramagnetic isomorph of Cr_2O_3, i.e., ruby, is well understood[8] so that the energy-level structure of the Cr^{3+} optical transitions is known. We already have a fairly detailed understanding of the $\vec{k} = 0$ excitons from our recent analysis of the optical spectrum, which has given a good picture of the interion exchange coupling. One consequence of the sizable (3–180 cm^{-1}) Davydov splittings observed[3,4] is that sublattice excitations are not at all close to being eigenstates. Another important property of the ^2E excitons which makes them an ideal case for study is that they couple only weakly to the lattice so we can, to a good approximation, neglect exciton-phonon coupling. This also enables us to observe the exciton-magnon transitions[9] without interference from exciton-phonon processes. These measurements will be used to support our model for the exciton dispersion.

To give some perspective, we briefly outline the situation with regard to exciton dispersion and Davydov splittings in solids other than magnetic insulators. In cases where interion (or intermolecule) coupling is strongest for translationally inequivalent ions a measurement of the Davydov splittings at $\vec{k} \simeq 0$ will essentially yield the total extent of the dispersion. Where this is not true the dispersion may be much larger than the Davydov splitting. The direct observation of dispersion requires the excitation of $\vec{k} \neq 0$ excitons. Because a photon probe has $\vec{k} \simeq 0$, excitons with large $\vec{k}$ can be observed only in situations where the initial or final state contains another excitation (usually a phonon or magnon) to conserve $\vec{k}$. The band shape of the combined excitation can, in principle, be analyzed for the exciton dispersion, if the dispersion of the added excitation and the transition matrix elements are known as a function of $\vec{k}$. This is, of course, much more indirect than the use of inelastic neutron scattering which is, however, restricted to low lying excitations with energy $\simeq kT$. An approximate measure of dispersion can sometimes be obtained by observing optical transitions in situations where the translational symmetry has been destroyed, for example by impurity substitution.

There have been a number of calculations of exciton dispersion in solids, for example in semiconductors[10] and alkali halides[11] where the excitons are of the Wannier type, and rare-gas[12] and organic solids[13,14] where they are of the Frenkel type. However, there are very few experimental data from which information on exciton dispersion can be obtained. The best examples are provided by organic molecular crystals where singlet excitons show large Davydov splittings and dispersion due to Coulomb interactions between the molecules. The strongly allowed (oscillator strength ~ 0.4) exciton in anthracene around 2500 Å shows a Davydov splitting of 16 000 cm^{-1},[15,16] and the weaker spin singlet around 3800 Å is split by 383 cm^{-1}.[17] In naphthalene the splitting of the 2000-Å singlet has not been measured, while the lowest singlet has a Davydov splitting of 166 cm^{-1}.[18] In both of these materials interactions between translationally inequivalent ions predominate, so the Davydov splittings give a good indication of the over-all dispersion of the singlet excitons. Further details of the exciton energy as a function of $\vec{k}$ in benzene and napthalene have recently been obtained by Colson *et al.*[19] by analyzing the band shape of exciton-phonon transitions involving essentially dispersionless optical phonons (molecular vibrations). Isotopic substitution which destroys translational symmetry has been used with some success to determine exciton dispersion in naphthalene.[20] For the lowest triplet (spin forbidden) excitons it has been proposed[14] that the electronic exchange interaction makes the dominant contribution to the dispersion and Davydov splittings. The latter are[21] 10 and[22] 22 cm^{-1} for the zero-phonon lines in naphthalene and anthracene, respectively.

In semiconductors, alkali halides, and rare-gas solids there do not appear to be experimental measurements of exciton dispersion although calculations have been made.[10–13] In these systems exciton-phonon (indirect) transitions are broad and often involve many phonons due to the strong coupling. This coupling considerably complicates the analysis of the zero-phonon structure for Davydov splittings and makes it essentially impossible to infer dispersion from the exciton-phonon absorption bands.

In Sec. II we review the relevant symmetry properties of the Cr_2O_3 lattice, the Brillouin zone, and the exciton states. In Sec. III we set up the eigenvalue problem and analyze the symmetry properties of the interion couplings. In Sec. IV we present expressions for the exciton dispersion and dispersion curves for several directions in $\vec{k}$ space. Experimental support of the dispersion calculation is provided by briefly analyzing the exciton-magnon band shape in Sec. V. A more detailed analysis of the exciton-magnon absorption will be published separately.

II. SYMMETRY PROPERTIES

Above its Néel temperature, Cr_2O_3 has the corundum structure D_{3d}^6 with two formula units per unit cell. The four chromium ions are at (c) sites of C_3 symmetry and the six oxygens are at (e) sites of C_2 symmetry.[23] Below T_N the magnetic symmetry group is D_{3d}^6 (D_3^7) and the unitary subgroup D_3^7 is symmorphic. The four Cr^{3+} spins labeled 1–4 (see Fig. 1) are collinear along the rhombohedral [111] axis and are ordered (+ − + −).[24] The rhombohedral cell is defined by $a_0 = 5.35$ Å and $\alpha = 55°9'$. For the direct lattice we can take the primitive translations to be[25]

$$\begin{aligned}\vec{T}_1 &= \quad s\vec{i} \qquad\quad + r\vec{k}\,,\\ \vec{T}_2 &= -\tfrac{1}{2}s\vec{i} + \tfrac{1}{2}\sqrt{3}\,s\vec{j} + r\vec{k}\,,\\ \vec{T}_3 &= -\tfrac{1}{2}s\vec{i} - \tfrac{1}{2}\sqrt{3}\,s\vec{j} + r\vec{k}\,,\end{aligned} \tag{2.1}$$

with $r = 4.55$ Å, $s = 2.816$ Å, and the volume of the unit cell equal to 96.2 Å^3. In D_{3d}^6 the nonprimitive translation $\vec{\tau}$ is $\frac{1}{2}(\vec{T}_1 + \vec{T}_2 + \vec{T}_3)$. Table I shows some important aspects of the geometry of Cr^{3+} ions which are near neighbors of a given Cr^{3+} ion up to the fourth nearest neighbor. The first, second, and third neighbors of a given ion have opposite spin and the fourth neighbor has the same spin, i.e., is ferromagnetically aligned.

In reciprocal space the primitive translation vectors are

$$\begin{aligned}\vec{K}_1 &= \quad s'\hat{i} \qquad\quad + r'\hat{k}\,,\\ \vec{K}_2 &= -\tfrac{1}{2}s'\hat{i} + \tfrac{1}{2}\sqrt{3}\,s'\hat{j} + r'\hat{k}\,,\\ \vec{K}_3 &= -\tfrac{1}{2}s'\hat{i} - \tfrac{1}{2}\sqrt{3}\,s'\hat{j} + r'\hat{k}\,,\end{aligned} \tag{2.2}$$

where $\hat{i}$, $\hat{j}$, $\hat{k}$ are unit vectors in $\vec{k}$ space and $r' = 2\pi/3r$, $s' = 4\pi/3s$. The Brillouin zone is shown in Fig. 2. The degeneracy and transformation properties of the exciton bands are determined by the zone symmetry and indicated by the representations of the groups of the $\vec{k}$ vector which are used as branch labels. The character tables for the groups of the $\vec{k}$ vector at Γ, Z, B, A and the lines Δ, Σ for D_{3d}^6 and D_3^7 are given by Slater[26] and will not be reproduced here. The $\vec{k} = 0$ group (at the point Γ) is isomorphic to the magnetic point group D_{3d} (D_3) whose unitary subgroup has representations A_1A_2 and E. We will sometimes use superscripts + and − to denote behavior under the operation RI of time reversal and space inversion which is an element of D_{3d} (D_3). The exciton labels at the special

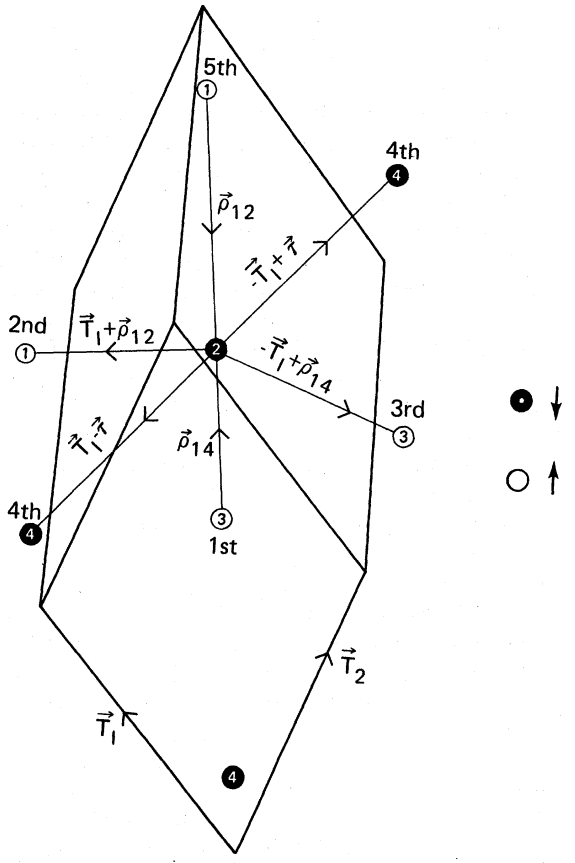

FIG. 1. Rhombohedral unit cell of Cr_2O_3 showing the spin arrangement and the neighbor geometry from the Cr^{3+} ion labeled No. 2 out to fifth nearest neighbors.

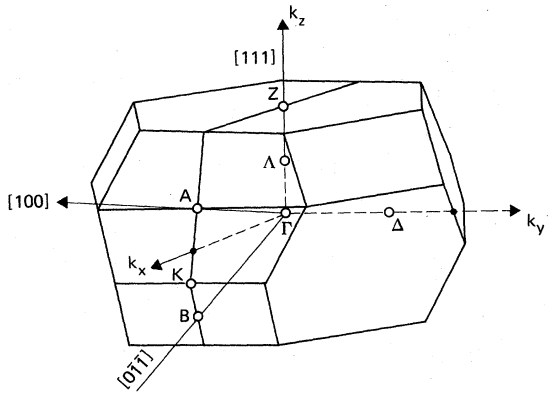

FIG. 2. Brillouin zone for Cr_2O_3 with high-symmetry points and lines marked. The irreducible zone has $\frac{1}{12}$ of this volume.

TABLE I. Geometry of near-neighbor Cr^{3+} ions.

Neighbor (and Dist. in Å)	Reference ion	Neighbor ion Type	(No.)	Vector Ref. → Neighbor	
first	1^+	4^-	(1)	$\vec{r}_1=\vec{\rho}_{14}$	
(2.65)	2^-	3^+	(1)	$-\vec{\rho}_{14}$	
	3^+	2^-	(1)	$\vec{\rho}_{14}$	
	4^-	1^+	(1)	$-\rho_{14}$	
second	1^+	2^-	(3)	$\vec{r}_2=\vec{T}_i+\vec{\rho}_{12}$	$i=1,2,3$
(2.89)	2^-	1^+	(3)	$-(\vec{T}_i+\vec{\rho}_{12})$	
	3^+	4^-	(3)	$\vec{T}_i+\vec{\rho}_{12}$	
	4^-	3^+	(3)	$-(\vec{T}_i+\vec{\rho}_{12})$	
third	1^+	4^-	(3)	$-(\vec{T}_i-\vec{\rho}_{14})$	$i=1,2,3$
(3.43)	2^-	3^+	(3)	$(\vec{T}_i-\vec{\rho}_{14})$	
	3^+	2^-	(3)	$-(\vec{T}_i-\vec{\rho}_{14})$	
	4^-	1^+	(3)	$\vec{r}_3=(\vec{T}_i-\vec{\rho}_{14})$	
fourth	1^+	3^+	(6)	$\vec{r}_4=\pm(\vec{T}_i-\vec{\tau})$	$i=1,2,3$
(3.65)	2^-	4^-	(6)	$\pm(\vec{T}_i-\vec{\tau})$	
	3^+	1^+	(6)	$\pm(\vec{T}_i-\vec{\tau})$	
	4^-	2^-	(6)	$\pm(\vec{T}_i-\vec{\tau})$	

points Γ, Z, B, and A are given in Table II. In Sec. III we will see that the symmetry properties impose useful restrictions on the form of the exciton states and the matrix elements of the exciton Hamiltonian.

III. EXCITON DISPERSION CALCULATION

A. Statement of Problem

The electronic Hamiltonian for the crystal can be written as a sum of single-ion and interion terms as

$$\mathcal{H}=\sum_{i=1}^{p}\sum_{n=1}^{N}\mathcal{H}(\vec{R}_{ni})+\sum_{\vec{R}_{ni}\neq\vec{R}_{mj}}\mathcal{H}(\vec{R}_{ni},\vec{R}_{mj})\,, \tag{3.1}$$

where $\vec{R}_{ni}$ is the position of the ith of p ions in the nth of N unit cells. The exact form of $\mathcal{H}$ will not be important here, except that it be invariant to the groups of $\vec{k}$ at all points in the Brillouin zone. The first term, $\mathcal{H}(\vec{R}_{ni})$, is essentially the ligand-field Hamiltonian for isolated Cr^{3+} ions, and in AMW an explicit form of $\mathcal{H}(\vec{R}_{ni},\vec{R}_{mj})$ is given, based on Anderson's[27] superexchange model for interion interactions.

We specify a subspace S of crystal states $|\mu\vec{R}_{ni}\rangle$ defined by an antisymmetrized product of localized states in which only the ion at $\vec{R}_{ni}$ is excited (to a single-ion state specified by μ), the others being in their ground states. We restrict our attention to two values of μ, i.e., $\mu_1\equiv t_2^{3\,2}E\tfrac{1}{2}a_4$ for spin-up ions labeled $i=1$ and 3, and the conjugate states $-\tfrac{1}{2}a_5$, for the spin-down ions 2 and 4, and $\mu_2\equiv t_2^{3\,2}E\tfrac{1}{2}a_6$ for $i=1$, 3 and $-\tfrac{1}{2}a_6$ for 2, 4. The C_{3v} double-group representations a_4, a_5, and a_6 are rigorous site labels, and $t_2^{3\,2}EM_s$ are approximate but the admixture of other terms is only about 10%. Since there are four Cr^{3+} ions per unit cell, this defines a subspace S of $8N$ states, and it is within this subspace that we diagonalize the Hamiltonian $\mathcal{H}$. Diagonal matrix elements of $\mathcal{H}$ in S for a given μ are equal, and off-diagonal elements are transfer-of-excitation (TOE) type connecting different ions. Specifically excluded are states with more than one ion excited,[28] as matrix elements to these are much less than the diagonal energy separation. The eigenvalue problem is then

$$\mathrm{Det}(\langle\mu R_{ni}|\mathcal{H}|\mu' R_{mj}\rangle-\lambda\langle\mu R_{ni}|\mu' R_{mj}\rangle)=0\,. \tag{3.2}$$

The states labeled by the other two values of μ for ^2E (viz., $-\tfrac{1}{2}a_5$ and $-\tfrac{1}{2}a_6$ for ions 1 and 3 and the conjugate states for ions 2 and 4) are also excluded from S since they give rise to higher-energy excitons involving nominally $\Delta M_s=2$ transitions from the ground state and these are not observed experimentally.

The symmetry of the crystal imposes certain conditions which simplify the solution of Eq. (3.2). For pairs of ions lying on the C_3 axis (e.g., first nearest neighbors) it is rigorously true that within S

TABLE II. Transformation properties of excitations in Cr_2O_3 [antiferromagnetic phase D_{3d}^6 (D_3^7)].

Γ point electric dipole selection	Γ	Z	A	B
–	A_1	Z_1	A_1	B_1
π	A_2	Z_2	A_2	B_2
σ	E	Z_3	A_1+A_2	B_1+B_2

$$\langle \mu R_{ni} | \mathcal{H} | \mu' R_{mj} \rangle \propto \delta_{\mu\mu'} , \tag{3.3}$$

i.e., TOE matrix elements between states which are not degenerate from ion to ion in zeroth order vanish. We assume that this is true for other ion pairs. This leads to a separate eigenvalue problem for each μ, i.e., two of order $4N$. Translational symmetry enables the formation of sublattice exciton states which transform irreducibly in the translation subgroup:

$$|\mu\vec{k}j\rangle = \frac{1}{\sqrt{N}} \sum_m e^{-i\vec{k}\cdot\vec{R}_{mj}} |\mu\vec{R}_{mj}\rangle$$

$$= \frac{1}{\sqrt{N}} e^{-i\vec{k}\cdot\vec{\rho}_j} \sum_m e^{-i\vec{k}\cdot\vec{T}_m} |\mu\vec{R}_{mj}\rangle , \tag{3.4}$$

where $\vec{T}_n$ are the primitive translations and $\vec{\rho}_j$ locates the jth ion in the unit cell. Matrix elements of $\mathcal{H}$ [which transforms identically in D_{3d}^6 (D_3^7)] are diagonal in $\vec{k}$:

$${}^{\mu}H_{ij}(\vec{k}) = \langle \mu\vec{k}i | \mathcal{H} | \mu\vec{k}j \rangle$$

$$= \sum_{m,n} e^{-i\vec{k}\cdot(\vec{R}_{mj}-\vec{R}_{ni})} \langle \mu\vec{R}_{ni} | \mathcal{H} | \mu\vec{R}_{mj} \rangle . \tag{3.5}$$

We further define for each μ

$${}^{\mu}h_{ij}^{(l)}(\vec{r}_l) = \langle \mu\vec{R}_{ni} | \mathcal{H} | \mu\vec{R}_{mj} \rangle , \tag{3.6}$$

where l denotes the neighbor (first, second, etc.) located by the relative vector $\vec{r} = \vec{R}_{mj} - \vec{R}_{ni}$. In a rhombohedral unit cell such as shown in Fig. 1, the vectors $\vec{\rho}_{ij}$ are parallel to the C_3 axis and connect ions i and j. The relative vectors for the first four neighbors are

$$\vec{r}_1 = \vec{\rho}_{14}, \quad \vec{r}_2 = \vec{T}_1 + \vec{\rho}_{12} , \quad \vec{r}_3 = \vec{T}_1 - \vec{\rho}_{14} , \quad \vec{r}_4 = \pm(-\vec{T}_1 + \vec{\tau}) ,$$

together with the vectors $\vec{r}_2'$, $\vec{r}_2''$, etc., generated from these by the operations C_3 and C_3^{-1}. The basic problem now is to diagonalize two 4×4 matrices at each $\vec{k}$, which corresponds to diagonalizing the intersublattice interactions.

At $\vec{k}=0$ the four states for $\mu=1$ transform according to a reducible representation $\Gamma_1 \rightarrow 2E$, and the four for $\mu=2$ as $\Gamma_2 \rightarrow 2(A_1+A_2)$. The linear combinations of the sublattice states which transform irreducibly at $\vec{k}=0$ can be expressed in the following transformation matrices (which can be deduced from AMW), where the rows are labeled by $\langle \mu, i|$:

$$\frac{1}{\sqrt{2}} \begin{array}{c} \\ \langle 1,1| \\ \langle 1,2| \\ \langle 1,3| \\ \langle 1,4| \end{array} \begin{array}{c} \begin{array}{cccc} E_\alpha^+ & E_\beta^+ & E_\alpha^- & E_\beta^- \end{array} \\ \begin{bmatrix} 0 & 1 & 0 & e^{i\phi} \\ e^{-i\phi} & 0 & -1 & 0 \\ 0 & e^{-i\phi} & 0 & -1 \\ 1 & 0 & e^{i\phi} & 0 \end{bmatrix} \end{array}$$

and

$$\frac{1}{2} \begin{array}{c} \\ \langle 2,1| \\ \langle 2,2| \\ \langle 2,3| \\ \langle 2,4| \end{array} \begin{array}{c} \begin{array}{cccc} A_1^+ & A_1^- & A_2^+ & A_2^- \end{array} \\ \begin{bmatrix} 1 & e^{i\phi_1} & 1 & e^{i\phi_2} \\ e^{-i\phi_1} & -1 & e^{-i\phi_2} & -1 \\ e^{-i\phi_1} & -1 & -e^{-i\phi_2} & 1 \\ 1 & e^{i\phi_1} & -1 & -e^{i\phi_2} \end{bmatrix} \end{array} , \tag{3.7}$$

and ϕ is the phase of ${}^1H_{13}(0)$, ϕ_1 of ${}^2H_{12}(0)+{}^2H_{13}(0)$, and ϕ_2 of ${}^2H_{12}(0)-{}^2H_{13}(0)$.

B. Symmetry Properties and Relationships between the $H_{ij}(\vec{k})$

A determination of the $H_{ij}(\vec{k})$ requires a calculation of the sum over pairs of ions in Eq. (3.5). In practice, because of the short range of the exchange interaction [which is the dominant term in $\mathcal{H}(\vec{R}_{ni}\vec{R}_{mj})$] the sum can be restricted to a few near neighbors. By going as far as the fourth neighbors ($l \le 4$) we include the nearest ones with the same spin as the reference ion. This is important since the largest TOE matrix element occurs between such ions. The geometry of the ion pairs is shown in Fig. 1 and Table I. The diagonal elements H_{ii} are equal and independent of $\vec{k}$. Most of the important ion-pair interactions which enter into the exciton dispersion also determine the $\vec{k}=0$ Davydov splittings which have been measured directly in the absorption spectrum. Therefore, with the model for the interactions which follows and the $\vec{k}=0$ energies, we get a good picture of the $\vec{k}$ dependence of the exciton energy bands.

Symmetry operations of the crystal, both unitary and antiunitary, impose certain restrictions on the ${}^{\mu}H_{ij}(\vec{k})$ and ${}^{\mu}h_{ij}^{(l)}(\vec{r}_l)$. First of all we look for relationships valid for general $\vec{k}$, and then we look in configuration space for conditions on particular ${}^{\mu}h_{ij}^{(l)}$ for a given neighbor type. The latter are, of course, consistent with the general $\vec{k}$-space result so that if ${}^{\mu}H_{ij}(\vec{k}) = {}^{\mu}H_{i'j'}(\vec{k})$ for all $\vec{k}$, then ${}^{\mu}h_{ij}^{(l)} = {}^{\mu}h_{i'j'}^{(l)}$ for all l. However, since we can restrict ourselves to a few values of l, more restrictive conditions on $h_{ij}^{(l)}$ can sometimes be found. The important results are summarized here and further details are given in the Appendix.

For the exciton branches derived from Γ_1 (i.e., $\mu=1$) we find

$${}^1H_{12}(\vec{k}) = c(\vec{k})\, {}^1h_{12}^{(2)}(\vec{r}_2)$$

and

$${}^1H_{34}(\vec{k}) = c(\vec{k})\, {}^1h_{12}^{(2)}(\vec{r}_2)^* ,$$

where

$$c(\vec{k}) = e^{i\vec{k}\cdot(\vec{T}_1+\vec{\rho}_{12})} + \omega e^{i\vec{k}\cdot(\vec{T}_2+\vec{\rho}_{12})} + \omega^2 e^{i\vec{k}\cdot(\vec{T}_3+\vec{\rho}_{12})}$$

$$(\omega = e^{2i\pi/3}),$$

$$^1H_{14}(\vec{k}) = {}^1H_{32}(\vec{k}) = {}^1h_{14}^{(3)}(-\vec{r}_3)\,(e^{-i\vec{k}\cdot(\vec{T}_1-\vec{\rho}_{14})} + \omega e^{-i\vec{k}\cdot(\vec{T}_2-\vec{\rho}_{14})} + \omega^2 e^{-i\vec{k}\cdot(\vec{T}_3-\vec{\rho}_{14})}),$$

$$^1H_{13}(\vec{k}) = {}^1H_{42}(\vec{k}) = 2\,{}^1h_{13}^{(4)}(\vec{r}_4)[\cos\tfrac{1}{2}\vec{k}\cdot(-\vec{T}_1+\vec{T}_2+\vec{T}_3) + \cos\tfrac{1}{2}\vec{k}\cdot(\vec{T}_1-\vec{T}_2+\vec{T}_3) + \cos\tfrac{1}{2}\vec{k}\cdot(\vec{T}_1+\vec{T}_2-\vec{T}_3)]. \quad (3.8)$$

Note that, at $\vec{k}=0$, $H_{12}(0)=H_{34}(0)=H_{14}(0)=H_{32}(0)=0$ and $H_{13}(0)=H_{42}(0)=6h_{13}^{(4)}$ as in AMW. Since the first-neighbor terms vanish, only interactions between ions of a single-near-neighbor type (within our limit of $l\le 4$) contribute to a given $^1H_{ij}(\vec{k})$. The largest TOE matrix element is the spin-allowed one $^1h_{13}^{(4)}$ which determines the $\vec{k}=0$ Davydov splitting of the E excitons. At this stage the assumption is made that at all $\vec{k}$ the spin-forbidden TOE matrix elements for second and higher neighbors can be neglected. The nearest-neighbor interaction, which in other symmetries would probably be the largest of these, vanishes by symmetry here. With this approximation the Γ_1 matrix at general $\vec{k}$

$$\mathcal{H}(\Gamma_1) = \begin{array}{c} \\ \langle 11| \\ \langle 12| \\ \langle 13| \\ \langle 14| \end{array} \begin{array}{c} \begin{array}{cccc} |11\rangle & |12\rangle & |13\rangle & |14\rangle \end{array} \\ \begin{bmatrix} E_1 & & & \\ {}^1H_{12}(\vec{k})^* & E_1 & & \\ {}^1H_{13}(\vec{k})^* & {}^1H_{14}(\vec{k}) & E_1 & \\ {}^1H_{14}(\vec{k})^* & {}^1H_{13}(\vec{k}) & {}^1H_{34}(\vec{k})^* & E_1 \end{bmatrix} \end{array} \quad (3.9)$$

becomes

$$\mathcal{H}(\Gamma_1) = \begin{array}{c} \\ \langle 11| \\ \langle 13| \\ \langle 14| \\ \langle 12| \end{array} \begin{array}{c} \begin{array}{cccc} |11\rangle & |13\rangle & |14\rangle & |12\rangle \end{array} \\ \begin{bmatrix} E_1 & & & \\ {}^1H_{13}(\vec{k})^* & E_1 & & \\ 0 & 0 & E_1 & \\ 0 & 0 & {}^1H_{13}(\vec{k})^* & E_1 \end{bmatrix} \end{array}, \quad (3.10)$$

where the matrices are Hermitian and only elements on and below the diagonal are shown. The approximation leading to Eq. (3.10) is also made because we do not have any information on the magnitude of the smaller TOE matrix elements. As methods are devised to get this information it can readily be included in the Γ_1-exciton-band Hamiltonian of Eq. (3.9). From the $\vec{k}=0$ energies in AMW we have $E_1 = 13835\ \mathrm{cm}^{-1}$ and $|h_{13}^{(4)}| = 15.3\ \mathrm{cm}^{-1}$.

For the excitons derived from $\Gamma_2(\mu=2)$, which reduces to $2(A_1+A_2)$ at $\vec{k}=0$, the situation is somewhat more complicated since none of the $H_{ij}(\vec{k})$ are rigorously zero. Symmetry considerations (see Appendix) lead to the following relationships:

$$^2H_{14}(\vec{k}) = {}^2H_{32}(\vec{k}) = {}^2h_{14}^{(1)}(\vec{r}_1)\,e^{i\vec{k}\cdot\vec{\rho}_{14}} + {}^2h_{14}^{(3)}(-\vec{r}_3) \times (e^{-i\vec{k}\cdot(\vec{T}_1-\vec{\rho}_{14})} + e^{-i\vec{k}\cdot(\vec{T}_2-\vec{\rho}_{14})} + e^{-i\vec{k}\cdot(\vec{T}_3-\vec{\rho}_{14})}),$$

$$^2H_{12}(\vec{k}) = {}^2H_{43}(-\vec{k}) = {}^2h_{12}^{(2)}(\vec{r}_2)\,(e^{i\vec{k}\cdot(\vec{T}_1+\vec{\rho}_{12})} + e^{i\vec{k}\cdot(\vec{T}_2+\vec{\rho}_{12})} + e^{i\vec{k}\cdot(\vec{T}_3+\vec{\rho}_{12})}).$$

If h_{12} and h_{43} are real, as is the case for magnons in Cr_2O_3,[29] then $H_{12}(\vec{k}) = H_{43}(\vec{k})$.

$$^2H_{13}(\vec{k}) = {}^2H_{42}(\vec{k}) = 2\,{}^2h_{13}^{(4)}(\vec{r}_4)[\cos\tfrac{1}{2}\vec{k}\cdot(-\vec{T}_1+\vec{T}_2+\vec{T}_3) + \cos\tfrac{1}{2}\vec{k}\cdot(\vec{T}_1-\vec{T}_2+\vec{T}_3) + \cos\tfrac{1}{2}\vec{k}\cdot(\vec{T}_1+\vec{T}_2-\vec{T}_3)]. \quad (3.11)$$

For the limiting case of $\vec{k}=0$, we have

$$^2H_{14}(0) = {}^2H_{32}(0) = {}^2h_{14}^{(1)}(\vec{r}_1) + 3\,{}^2h_{14}^{(3)}(-\vec{r}_3),$$

and is real. Further,

$$^2H_{12}(0) = {}^2H_{43}(0) = 3\,{}^2h_{12}^{(2)}(\vec{r}_2),$$

$$^2H_{13}(0) = {}^2H_{42}(0) = 6\,{}^2h_{13}^{(4)}(\vec{r}_4),$$

which is consistent with the conditions imposed by the factor group, as it must be. The form of $\mathcal{H}(\Gamma_2)$ for general values of $\vec{k}$ is then

$$\mathcal{H}(\Gamma_2) = \begin{array}{c} \\ \langle 21| \\ \langle 22| \\ \langle 23| \\ \langle 24| \end{array} \begin{array}{c} \begin{array}{cccc} |21\rangle & |22\rangle & |23\rangle & |24\rangle \end{array} \\ \begin{bmatrix} E_2 & & & \\ {}^2H_{12}(\vec{k})^* & E_2 & & \\ {}^2H_{13}(\vec{k})^* & {}^2H_{14}(\vec{k}) & E_2 & \\ {}^2H_{14}(\vec{k})^* & {}^2H_{13}(\vec{k}) & {}^2H_{12}(-\vec{k}) & E_2 \end{bmatrix} \end{array}. \quad (3.12)$$

A more convenient form which shows the relationship to the $\vec{k}=0$ Hamiltonian is obtained by transforming Eq. (3.12) to get $\mathcal{H}(\Gamma_2)' = S^{-1}\mathcal{H}(\Gamma_2)S$, where

$$S = \frac{1}{\sqrt{2}} \begin{bmatrix} 1 & 0 & 1 & 0 \\ 0 & 1 & 0 & 1 \\ 0 & 1 & 0 & -1 \\ 1 & 0 & -1 & 0 \end{bmatrix},$$

and clearing over-all phases. Then

$$\mathcal{H}(\Gamma_2)' = \begin{bmatrix} E_2 + h_{14}^{(1)} \cos \vec{k}\cdot\vec{\rho}_{14} & & & \\ |h_{12}^{(2)}|\, Y(\vec{k}) & E_2 + h_{14}^{(1)} \cos \vec{k}\cdot\vec{\rho}_{14} & & \\ +2e^{-i\Delta\phi} h_{13}^{(4)} W(\vec{k}) & & & \\ h_{14}^{(1)} \sin \vec{k}\cdot\vec{\rho}_{14} & |h_{12}^{(2)}|\, X(\vec{k}) & E_2 - h_{14}^{(1)} \cos \vec{k}\cdot\vec{\rho}_{14} & \\ |h_{12}^{(2)}|\, X(\vec{k}) & h_{14}^{(1)} \sin \vec{k}\cdot\vec{\rho}_{14} & -|h_{12}^{(2)}|\, Y(\vec{k}) & E_2 - h_{14}^{(1)} \cos \vec{k}\cdot\vec{\rho}_{14} \\ & & +2e^{-i\Delta\phi}|h_{13}^{(4)}|\, W(\vec{k}) & \end{bmatrix}, \qquad (3.12')$$

where $h_{14}^{(3)}$, the third-neighbor coupling, has been neglected compared to $h_{14}^{(1)}$. The phase $\Delta\phi = \phi_{12} - \phi_{13}$ is the difference between the phases of the matrix elements ${}^2h_{12}^{(2)}$ and ${}^2h_{13}^{(2)}$. An analysis of the $\vec{k} = 0$ exciton g values in AMW suggested that $|\phi_1 - \phi_2| = \pi$ [see after Eq. (3.7) for the definition of ϕ_1, ϕ_2]. It can be shown from this that $e^{i\Delta\phi}$ is real and that $\Delta\phi = \pi$ is consistent with the $\vec{k} = 0$ energies. Since $h_{14}^{(1)}$ is real, the matrix of $\mathcal{H}(\Gamma_2)'$ is real. The $\vec{k}$-dependent factors not given explicitly above are

$$X(\vec{k}) = \sin \vec{k}\cdot(\vec{T}_1 + \vec{\rho}_{12}) + \sin \vec{k}\cdot(\vec{T}_2 + \vec{\rho}_{12}) + \sin \vec{k}\cdot(\vec{T}_3 + \vec{\rho}_{12}),$$

$$Y(\vec{k}) = \cos \vec{k}\cdot(\vec{T}_1 + \vec{\rho}_{12}) + \cos \vec{k}\cdot(\vec{T}_2 + \vec{\rho}_{12}) + \cos \vec{k}\cdot(\vec{T}_3 + \vec{\rho}_{12}),$$

$$W(\vec{k}) = \cos \tfrac{1}{2}\vec{k}\cdot(-\vec{T}_1 + \vec{T}_2 + \vec{T}_3) + \cos \tfrac{1}{2}\vec{k}\cdot(\vec{T}_1 - \vec{T}_2 + \vec{T}_3) + \cos \tfrac{1}{2}\vec{k}\cdot(\vec{T}_1 + \vec{T}_2 - \vec{T}_3). \qquad (3.13)$$

At $\vec{k} = 0$, $X(0) = 0$ so the off-diagonal block vanishes and we have the A_1 and A_2 blocks on the diagonal as expected. The approximation made for the Γ_1 branches of neglecting nominally spin-forbidden TOE between second and farther neighbors [i.e., $H_{12}(\vec{k}) = 0$] could also be consistently made here. However, $H_{12}(\vec{k})$ contributes to the $\vec{k} = 0$ Davydov splitting between the A_1^- and A_2^- branches, which has been measured experimentally.[3] Our previous analysis of the $\vec{k} = 0$ energies[4] gives $E_2 = 13827$ cm^{-1}, $|h_{13}^{(4)}| = 10.6$ cm^{-1}, $h_{14}^{(1)} = -8.5$ cm^{-1}, and $|h_{12}^{(2)}| = 2.2$ cm^{-1}. The $\vec{k}$ dependence of the matrix elements of $\mathcal{H}(\Gamma_2)'$ is shown explicitly in Eqs. (3.12′) and (3.13) so all of the quantities necessary to calculate the Γ_2 exciton band structure are known.

IV. EXCITON BANDS

The final diagonalization of the Γ_1 exciton Hamiltonian in the approximation of Eq. (3.10) is very simple, and the eigenvalues for all $\vec{k}$ are

$$\lambda_{1,2}(\Gamma_1) = E_1 \pm |{}^1H_{13}(\vec{k})|. \qquad (4.1)$$

Because of the simple 2×2 form resulting from the retention of only spin-allowed TOE matrix elements, the eigenvectors of (Γ_1) are not $\vec{k}$ dependent, and are the same as those given in the first matrix of Eq. (3.7). The eigenvalues depend only on the magnitude of ${}^1H_{13}$ and ${}^1h_{13}^{(4)}$, whereas the phase of ${}^1H_{13}$ comes into the eigenvectors but, as we have observed, it is not a $\vec{k}$-dependent phase. Using the values of $E_1 = 13835$ cm^{-1} and $|{}^1h_{13}^{(4)}| = 15.3$ cm^{-1} obtained from the $\vec{k} = 0$ energies, we obtain the $\vec{k}$-dependent eigenvalues $\lambda_{1,2}$ which are plotted in Fig. 3 for five directions in the Brillouin zone (of Fig. 2). The only place in the zone (apart from $\vec{k} = 0$) where the Γ_1 branches are required to be degenerate for a most general Hamiltonian is at the Z point where they transform like $2Z_3$ (Z_3 being doubly degenerate). The bands of Eq. (4.1) show a fourfold degeneracy at Z and A which occurs because the Hamiltonian of Eq. (3.10) has higher symmetry than D_{3d}^6 (D_3^7). Inclusion of ${}^1H_{12}$, ${}^1H_{34}$, and ${}^1H_{14}$ would produce a small change in the band energies, and a small splitting of the degenerate bands at the zone-boundary points A and Z.

For the four Γ_2 branches the approximation of neglecting the nominally spin-forbidden TOE for neighbors farther than the first $[H_{12}(\vec{k}) = 0]$ results in a simple analytical form for the eigenvalues of Eq. (3.12), i.e.,

$$\lambda_{1,2,3,4}(\Gamma_2) = E_2 \pm |{}^2H_{13}(\vec{k})| \pm |{}^2H_{14}(\vec{k})|. \qquad (4.2)$$

Analytical expressions for the vectors can also be obtained, and these are $\vec{k}$ dependent, as well as depending on the phase of ${}^2h_{13}$. The Davydov splitting between the A_1^+, A_2^+ and A_1^-, A_2^- branches at $\vec{k} = 0$ is then $2|H_{14}|$ or 17 cm^{-1}. However, as noted in Sec. III, we know the A_1^-, A_2^- Davydov splitting (3.5 cm^{-1}),[3] and a lower limit (25 cm^{-1}) for the A_1^+, A_2^+ Davydov splitting.[4] This fixes $|{}^2h_{12}^{(2)}| = 2.2$ cm^{-1} and enables us to solve the more general form, $\mathcal{H}(\Gamma_2)'$, whose eigenvalues for a number of directions in $\vec{k}$ space are plotted in Fig. 3, together with those of $\mathcal{H}(\Gamma_1)$. For our choice of $\Delta\phi = \pi$, all the matrix elements of $\mathcal{H}(\Gamma_2)'$ are real and it can readily be transformed into two 2×2 blocks. Inspection of Table II shows that, in general, the four Γ_2

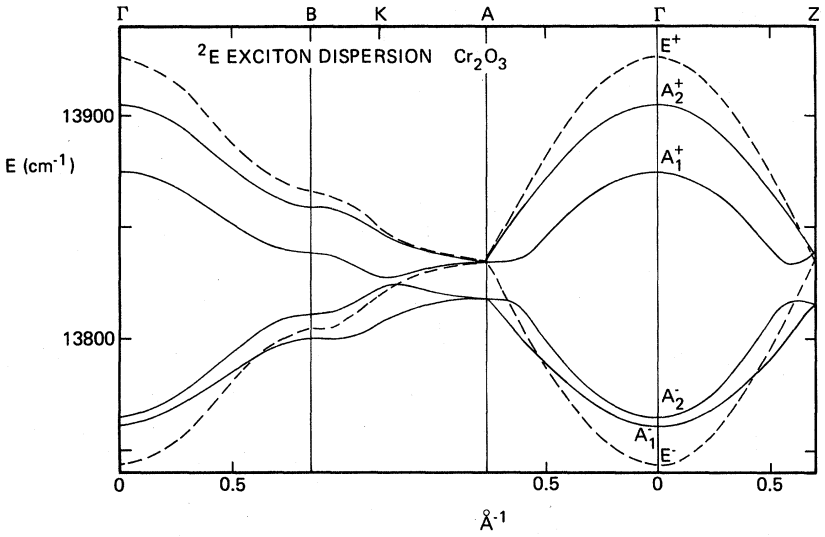

FIG. 3. Calculated exciton dispersion curves for the lowest eight branches of the ^2E excitons in a number of directions in the Brillouin zone. The $k=0$ labels are shown and the transformation properties at some other special points can be seen from Table II. The dotted curves are the Γ_1 excitons, and the solid curves Γ_2. Branches which become degenerate at special points can have nonzero slope at the zone boundary, e.g., the slope of the E^+ and E^- branches at the Z and A points is $\mp 3\gamma |\,^1h_{13}|$ or ∓ 208 cm^{-1}/Å^{-1}.

branches will be nondegenerate throughout the zone. However, we again find extra degeneracy at the Z and A points. The eigenvectors of $\mathcal{H}(\Gamma_2)'$ are $\vec{k}$ dependent, as noted above. For example, at $\vec{k}=0$, A_1^- has the vector $(\frac{1}{2},\frac{1}{2},\frac{1}{2},\frac{1}{2})$ and at $\vec{k}=\pi/c$, $(0.635,\ 0.635,\ -0.311,\ -0.311)$, in terms of the basis states of Eq. (3.12).

The exciton density of states

$$\rho^{ex}(E)=\sum_{\vec{k}}\delta(E-E^{ex}_{\vec{k}})$$

was calculated using a Monte Carlo algorithm and a mesh of $n=10^5$ points in the irreducible $\frac{1}{12}$ of the Brillouin zone. Several calculations were made, varying the number of points in the mesh. The statistical noise fluctuations on $\rho(E)$ depend on the number of points in a given energy interval, but are proportional to $n^{-1/2}$, and were less than ~5% for $n=10^5$. Figure 4 shows the result obtained using an energy resolution of 1 cm^{-1}.

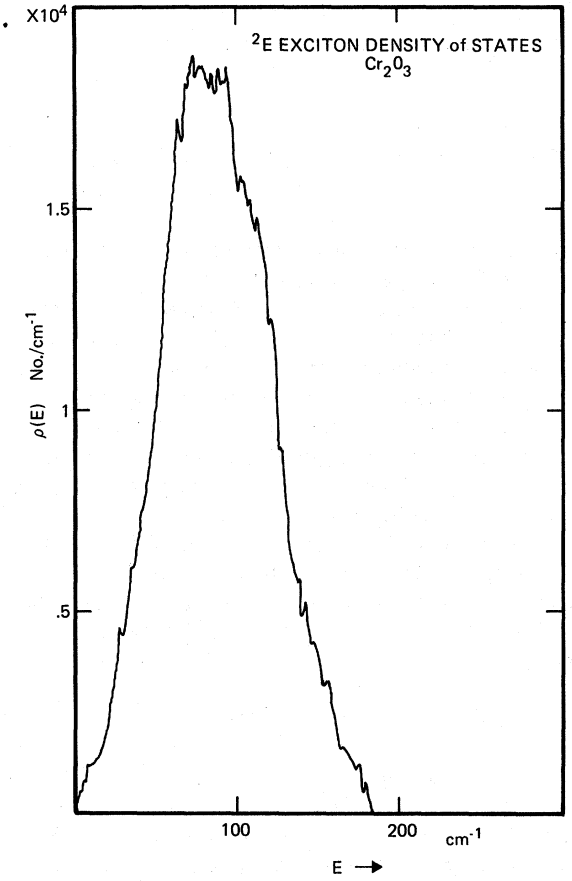

FIG. 4. Density of states of the excitons shown in Fig. 3. This was calculated using a Monte Carlo algorithm and a channel width of 1 cm^{-1}.

V. EXCITON-MAGNON ABSORPTION AS CONFIRMATION OF EXCITON DISPERSION

As pointed out in the Introduction, an optical measurement of exciton dispersion involving the creation of excitons with all values of $\vec{k}$ requires another quasiparticle to be excited for $\vec{k}$ conservation. We have obtained experimental support for our model of exciton dispersion by measuring the exciton-magnon absorption associated with the eight ^2E exciton branches whose dispersion was calculated in Sec. IV. It will be sufficient for our present purpose to give a preliminary analysis of the σ polarized exciton-magnon absorption as this is related in a simpler way to the exciton density of states. The π polarized spectrum and an extended treatment of the exciton-magnon band shapes will be covered in a future publication.

The experimental spectrum was measured at 1.6 °K using a single crystal of Cr_2O_3 2×2 mm polished to 15-μ thickness, with the c axis in the plane. The crystal was cemented to a sapphire

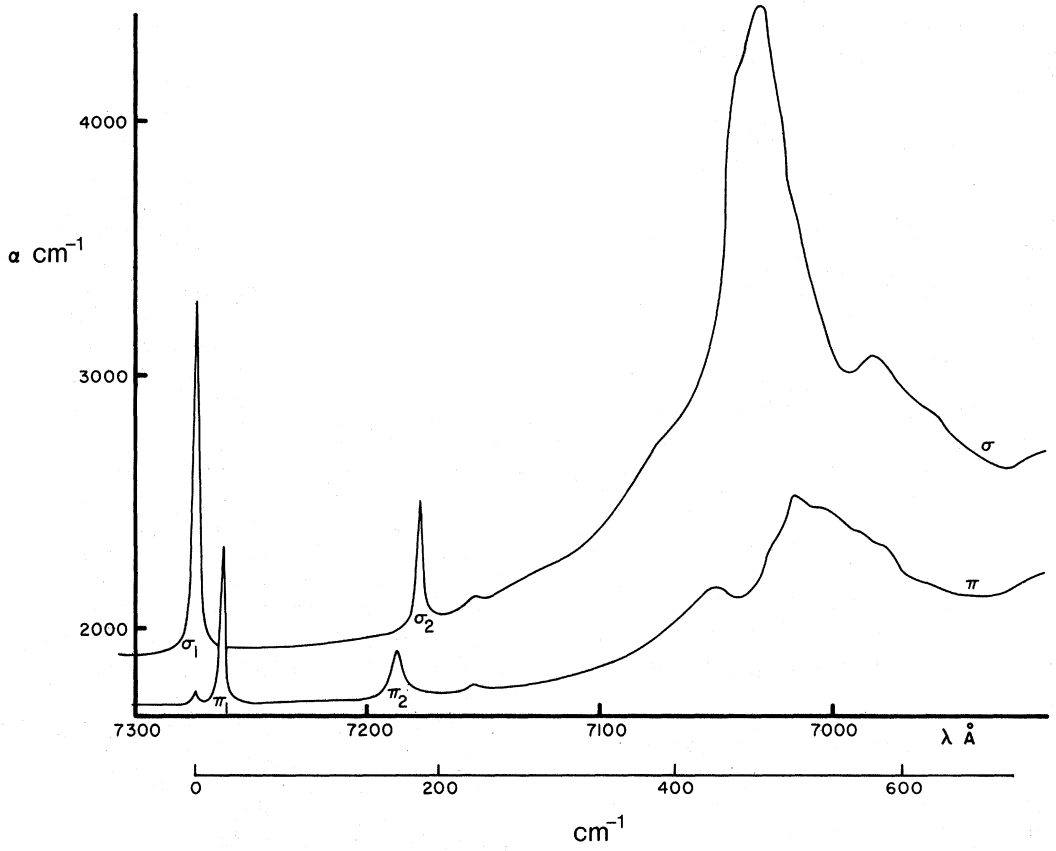

FIG. 5. Polarized exciton-magnon absorption bands in Cr_2O_3 at 2 °K.

substrate with its c axis parallel to that of the Cr_2O_3. No strain broadening was observed over and above that present in thicker freely suspended samples. The spectra were recorded digitally, point by point, by an IBM 1800 process control computer and the ratio to the incident light intensity calculated numerically. This gave the absorption coefficient and corrected for the energy dependence of the spectrometer and detector response. Figure 5 shows the σ and π polarized spectra. A comparison of the σ, π, and axial spectra (the latter taken with a different crystal) showed that the observed spectra arise from electric dipole transitions. In Table III are listed the absorption cross sections. The excitons are nominally spin and parity forbidden and get most of their intensity at $T=0$ from the single-ion mechanisms of the spin-orbit interaction mixing $t_2^2e\,{}^4T_2$ into $t_2^{3\,2}E$, and the odd parity crystal-field mixing charge transfer and $3d^3$ states (as in the case of ruby). The exciton-magnon transitions are more allowed since, in addition to these mechanisms, the interion exchange interaction also enables spin and parity to be conserved.[30] Phonon sidebands are ruled out as a possible origin of the observed spectra since the ^2E level couples very weakly to the lattice, and the exciton-phonon absorption would have about the same intensity relative to the pure exciton absorption, as is observed in ruby, i.e., less than $\frac{1}{2}$.

The microscopic mechanism for exciton-magnon absorption[30] involves a two-center excitation in which an ion at $\vec{R}_{ni}$ is excited to an optical state μ (which labels exciton branches), and an ion at $\vec{R}_{mj}$ is excited within the ground-state manifold, in this case $^4A_2$, to the state ν (which labels magnon branches). Let ρ_{ij}^m be the vector which locates the spin deviation on ion j in cell m relative to the optically excited ion. Then the exciton-magnon state at $\vec{k}=0$ (which can be excited by a photon) can be written

$$|\mu,-\vec{k};\nu,\vec{k}\rangle=\frac{1}{N}\sum_{ij}\sum_{nm}e^{-i\vec{k}\cdot\vec{\rho}_{ij}^m}\times Q_{i\mu}(-\vec{k})\,S_{j\nu}(\vec{k})\,|\vec{R}_{ni},\vec{\rho}_{ij}^m\rangle\ . \quad (5.1)$$

Q and S are the eigenvector matrices of the exciton and magnon Hamiltonians, respectively. The integrated absorption cross section (per chromium ion) in polarization ϵ, for the exciton-magnon transitions from the crystal ground state $|G\rangle$ in

TABLE III. Measured absorption cross sections for ^2E exciton and exciton-magnon transitions in Cr_2O_3 ($T = 1.6$ °K).

Transition		Peak α (cm^{-1})	Cross section/Cr^{3+} ion $\frac{1}{4N}\int \alpha(E)dE$ (10^{-20} cm)
exciton	σ_1	1350	27
	π_1	600	20
	π_2	170	11
	σ_2	500	16
exciton-magnon	σ	2100	580
	π	650	210

the absence of exciton-magnon interaction is[31]

$$\left[\frac{1}{4N}\int \alpha(E)\,dE\right]_\epsilon = \frac{8\pi^3 E}{hc}\left(\frac{\eta^2+2}{3\eta}\right)^2 \sum_{\vec{k}} \sum_{\mu,\nu} |\langle \mu, -\vec{k}; \nu, \vec{k}|\, P_\epsilon |\, G\rangle|^2 \times \delta[E - E_{ex}(\mu, -\vec{k}) - E_{mag}(\nu, \vec{k})], \quad (5.2)$$

where E is the transition energy in cm^{-1}, ϵ labels the components of the dipole operator P, and the refractive index (η) function is an approximate local-field correction. From Eqs. (5.1) and (5.2) we have for the integrated absorption coefficient

$$\left[\frac{1}{4N}\int \alpha(E)\,dE\right]_\epsilon = \frac{8\pi^3 E}{hc}\left(\frac{\eta^2+2}{3\eta}\right)^2 \sum_{\vec{k}} \sum_{\mu,\nu} \sum_{\substack{i,i'\\ j,j'}} \sum_{m,m'} Q_{i\mu}(-\vec{k})\, Q^*_{i'\mu}(-\vec{k}) \times S_{j\nu}(\vec{k})\, S^*_{j'\nu}(\vec{k})\, e^{i\vec{k}\cdot\vec{\rho}^m_{ij}}\, e^{-i\vec{k}\cdot\vec{\rho}^{m'}_{i'j'}}\, F_\epsilon(\vec{\rho}^m_{ij})\, F_\epsilon(\vec{\rho}^{m'}_{i'j'}) \times \delta[E - E_{ex}(\mu, -\vec{k}) - E_{mag}(\nu, \vec{k})]. \quad (5.3)$$

The F's are two-site transition moments which depend on the particular pair of ions excited—one being ion i in a reference unit cell, and the other being ion j in unit cell m. Equation (5.3) is expressed in a way that makes clear what the exciton-magnon band shape depends on, and the meaning of certain approximations which we will proceed to make in order to simplify the analysis. First we note that Eq. (5.3) has the form of a weighted convolution of the exciton-magnon density of states in which the exciton and magnon have equal and opposite wave vector. The weighting factors can be divided into $\vec{k}$-dependent ones—arising from the mode vectors (Q's and S's), the exponential factors, and the exciton and magnon dispersion—and branch-dependent ones. The latter are the intrinsic phases of the exciton mode vectors *relative to the magnons*, i.e., ϕ, ϕ_1, and ϕ_2 of Eq. (3.7). As we have seen, only the difference $\phi_1 - \phi_2$ effects the exciton energies. Since the exciton and magnon have linewidths at $T = 0$ of less than 3 cm^{-1}, we neglect relaxation and strain broadening of the exciton-magnon band shape. Selection rules on the symmetry of excitons and magnons which can contribute to polarized exciton-magnon absorption are not very restrictive. For sidebands of the Γ_1 exciton branches, contributions from all special (and, of course, general) points are allowed. For the Γ_2 branch, all points are allowed except the Z point which is forbidden in π absorption.

In the presence of a number of approximations, which we now state, the σ polarized exciton-magnon band shape is given simply by the joint density of states; i.e., the $\vec{k}$-dependent and branch-dependent weighting factors can be neglected. The approximations are as follows:

(i) Exciton-magnon interaction can be neglected. This is a reasonable first step introduced to simplify the analysis at this stage.

(ii) The dominant absorption mechanism involves nearest-neighbor Cr^{3+} ion pairs ($\vec{\rho}^m_{ij} \equiv \vec{\rho}^0_{14}$). This is physically reasonable since they are the closest ions, and they have opposite spin and hence can satisfy $\Delta M_s = 0$ in the electric dipole transition. Further, these pairs lie along the C_3 axis and give rise to $\vec{k} = 0$ exciton-magnon states of E symmetry[32] which are electric dipole active only in σ polarization. Experimentally, the σ polarized absorption is about three times stronger than π (which arises from excitation of more distant neighbor pairs).

(iii) The exciton and magnon mode vectors Q and S are $\vec{k}$ independent. This is true near the zone boundaries where the density of states is high, and so is probably a fair assumption.

(iv) All branches of the ^2E excitons couple to the magnons with equal probability. This is hard to justify *a priori* and we will comment on it further below.

In the light of the above approximations, we calculate the combined exciton-magnon density of states

$$\rho^{e\text{-}m}(E) = \sum_{\vec{k},\mu,\nu} \delta[E - E_{ex}(\mu, -\vec{k}) - E_{mag}(\nu, \vec{k})]$$

using expressions for the magnon dispersion given by Samuelsen[29] and by Alikhanov *et al.*[33] (fitted to inelastic-neutron-scattering data[33,34]) and our Eq. (4.1) and the solutions of Eq. (3.12′) for the excitons. In Fig. 6 $\rho^{e\text{-}m}(E)$ is compared with the experimental exciton-magnon σ band shape and the agreement is seen to be quite good. To show the dependence of the calulated band shape on the exciton dispersion, we have also calculated the joint ex-

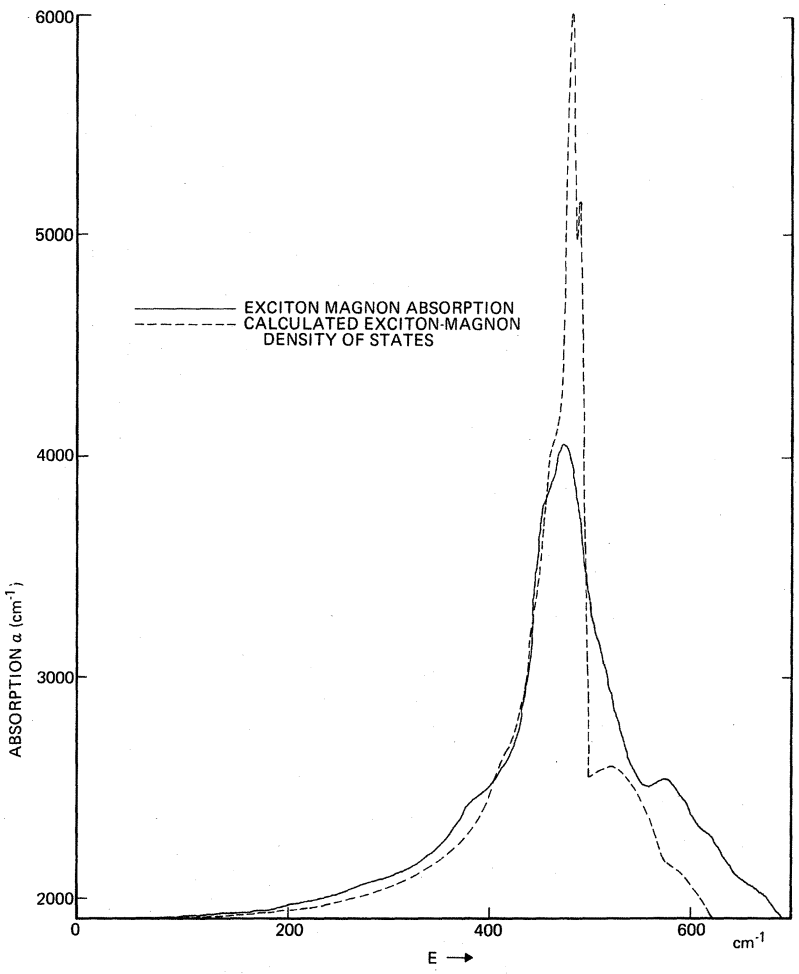

FIG. 6. Comparison of the σ polarized exciton-magnon absorption spectrum measured at 2 °K with the calculated exciton-magnon density of states. The area under the joint density of states is equal to that of the integrated exciton-magnon absorption. The channel width for the calculation was 1 cm^{-1} and the experimental spectral resolution was 1 cm^{-1}.

citon-magnon density of states for dispersionless excitons and this is shown in Fig. 7. These results support the over-all features of our exciton dispersion calculation, although some changes in the model may be required as further information bearing on the excitons and their dispersion becomes available. For example, recent exciton absorption data by Allen[35] through the spin-flopped configuration suggest that the upper A_2^+ branch may have been incorrectly assigned in AMW and may instead lie above the upper E branch.

By making the approximations listed above, we were able to calculate a band shape with no adjustable parameters—those describing the exciton dispersion having been determined separately. The assumption that the branch-dependent weighting factors (which are functions of ϕ, ϕ_1, and ϕ_2) are equal is probably the weakest point. Information on these phases can be obtained from the relative intensities of the $\vec{k}=0$ excitons as was done recently for $YCrO_3$ by Meltzer.[6] Such refinements are currently being incorporated into an extension of the band-shape calculation.

VI. CONCLUSION

Although exciton dispersion in magnetic insulators is probably fairly widespread, only one previous example of experimental evidence for it seems to have been recorded. That is the negative dispersion in the $^4A_1$, ^4E branches of MnF_2 which results in an exciton-magnon band with lower energy than the exction.[7] The origin of dispersion is the interaction between magnetic ions which we believe to be largely of the exchange type. In situations where the excitons couple strongly to phonons the TOE matrix elements will be reduced by vibrational overlap factors, and exciton dispersion will be considerably reduced. This is probably the reason for the negligible dispersion of the $^4T_1$ excitons in MnF_2, for example.[36] The ^2E excitons in Cr_2O_3 provide one of the best cases for study since the transition involves relatively simple single-ion states and the coupling to phonons is very weak.

We have fully exploited the symmetry properties of the crystal to reduce the number of independent two-center Coulomb and exchange integrals (the

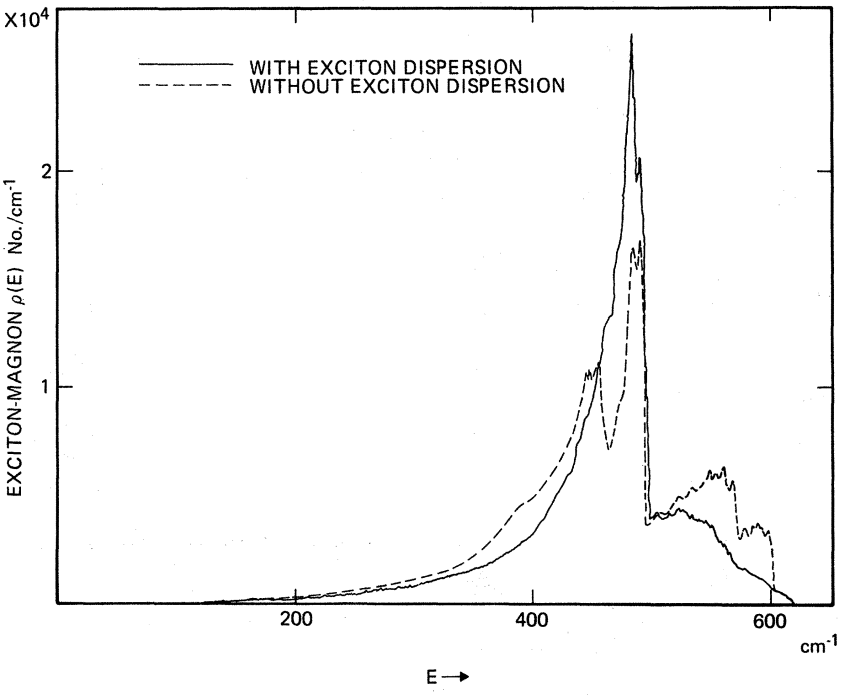

FIG. 7. Comparison of the exciton-magnon density of states with and without exciton dispersion. This is shown to illustrate the dependence of the exciton-magnon density of states (and hence the exciton-magnon absorption band shape) on the exciton dispersion.

h's) which enter into the dispersion calculation. These integrals are treated as empirical parameters and most of them are obtainable from our earlier analysis of the $\vec{k}=0$ energies. A number of approximations have been made, and these can be removed as more information on the details of exciton dispersion become known. For example, we diagonalize the exciton Hamiltonian within the set of states which are degenerate from ion to ion in zeroth order (zeroth order including diagonal exchange only—no TOE). Nonresonant TOE may be important, and its inclusion would lead to energy matrices of order pN for transfer between p different single-ion levels. This introduces a large number of unknown matrix elements and phases, and a systematic calculation scheme which keeps track of the relative phases of the single-ion levels will have to be developed to deal with the pairwise interactions (cf. the tensor-operator techniques in atomic and crystal-field theory).

Since direct measurement of the E-vs-$\vec{k}$ relationship of optical excitons is not possible, it is more difficult to obtain information on the details of the exciton-band structure, compared to the case for magnons or phonons where inelastic neutron scattering can be used. However, we have obtained confirmation that at least the main features of our exciton-band calculation are correct, by measuring the exciton-magnon absorption band shape and comparing it to a numerical computation of the joint exciton-magnon density of states.

APPENDIX

The symmetry restrictions on the $H_{ij}(\vec{k})$ are explored in further detail here. Let Θ_u and Θ_a be unitary and antiunitary operators of the magnetic space group—in this case $D_{3d}^6(D_3^7)$. Then Θ_u and Θ_a commute with the Hamiltonian $\mathcal{H}$ so that

$$\langle i|\mathcal{H}|j\rangle = \langle \Theta_u i|\mathcal{H}|\Theta_u j\rangle \tag{A1}$$

and

$$\langle i|\mathcal{H}|j\rangle = \langle \Theta_a i|\mathcal{H}|\Theta_a j\rangle^* . \tag{A2}$$

We are, therefore, interested in the transformation properties of the basis states under Θ_u and Θ_a. For the Γ_1 excitons, the functions $|j\rangle$ transform like a_3 of the group C_3 for $j=1$, 3 and a_2 for $j=2$, 4. For the Γ_2 excitons all $|j\rangle$ transform like the identity a_1.

A. Relations in k Space

Sublattice exciton states

$$|i\vec{k}\rangle = N^{-1/2}\sum_n e^{-i\vec{k}\cdot\vec{R}_{ni}}|\vec{R}_{ni}\rangle \tag{A3}$$

transform under Θ_u as follows:

$$\Theta_u|i\vec{k}\rangle = N^{-1/2}\sum_n\sum_m e^{-i\vec{k}\cdot\vec{R}_{ni}}\langle\vec{R}_{mj}|\Theta_u|\vec{R}_{ni}\rangle|\vec{R}_{mj}\rangle , \tag{A4}$$

but

$$\langle\vec{R}_{mj}|\Theta_u|\vec{R}_{ni}\rangle = e^{i\chi_m(\Theta_u)} \quad \text{if} \quad \vec{R}_{ni} = \Theta_u^{-1}\vec{R}_{mj}$$

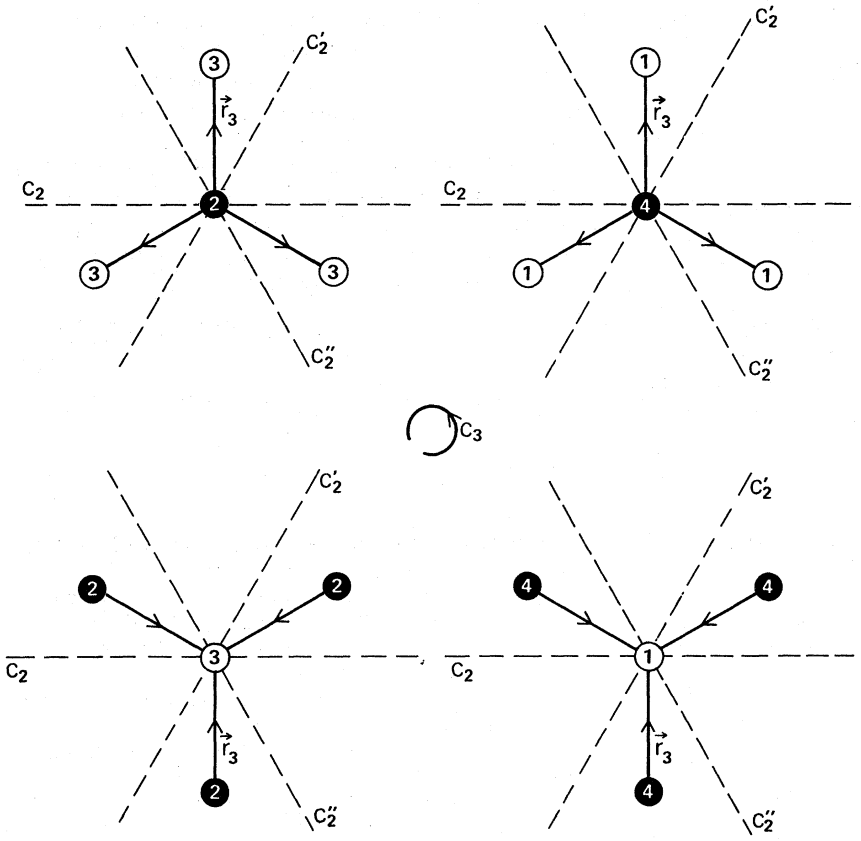

FIG. 8. Local geometry for third neighbors of ions of each sublattice type, viewed down the C_3 axis. The arrows on the relative vectors point out of the page.

$= 0$ otherwise . (A5)

The phase angle $\chi_m(\Theta_u)$ is determined by the rotational properties of the site functions. Therefore,

$$\Theta_u|i\vec{k}\rangle = N^{-1/2}\sum_m e^{i\chi_m(\Theta_u)}\, e^{-i(\Theta_u\vec{k})\cdot\vec{R}_{mj}}|\vec{R}_{mj}\rangle \ . \tag{A6}$$

Similarly for the antiunitary operators

$$\Theta_a|i\vec{k}\rangle = N^{1/2}\sum_m e^{i\chi_m(\Theta_a)}\, e^{i(\Theta_a\vec{k})\cdot\vec{R}_{mj}}|\vec{R}_{mj}\rangle \ . \tag{A7}$$

The useful $\vec{k}$-space relationships are as follows:

(a) At general $\vec{k}$, RI (the operation of time reversal $\times$ space inversion) is the only symmetry operation (i.e., $RI\vec{k}\equiv\vec{k}$), and it interchanges sublattices $1 \rightleftharpoons 2$ and $3 \rightleftharpoons 4$. We can take $\chi_m(RI) = 0$ so that Eqs. (A2) and (A7) give

$$\left.\begin{aligned} {}^{\mu}H_{13}(\vec{k}) &= {}^{\mu}H_{42}(\vec{k}) \\ {}^{\mu}H_{14}(\vec{k}) &= {}^{\mu}H_{32}(\vec{k}) \end{aligned}\right\} \quad \text{for } \mu = 1, 2 \ . \tag{A8}$$

(b) The operation C_2 takes $\vec{k} \rightarrow -\vec{k}$ and interchanges sublattices $1 \rightleftharpoons 4$ and $2 \rightleftharpoons 3$. In this case $\chi_m(C_2)$ is zero only for the Γ_2 excitons. Then Eqs. (A1) and (A6) yield

$${}^{2}H_{12}(\vec{k}) = {}^{2}H_{43}(-\vec{k}) \ . \tag{A9}$$

B. Relations in Configuration Space

In configuration space there are a number of useful relationships among the ${}^{\mu}h_{ij}^{(l)}$ of Eq. (3.6). For first neighbors ($l = 1$) which lie along the C_3 axis Eq. (A1) gives for $\mu = 1$

$$\langle i|\mathcal{H}|4\rangle = \langle C_3 1|\mathcal{H}|C_3 4\rangle = e^{i4\pi/3}\langle 1|\mathcal{H}|4\rangle \ , \tag{A10}$$

with a similar expression for $\langle 2|\mathcal{H}|3\rangle$. Therefore,

$${}^{1}h_{14}^{(1)} = {}^{1}h_{23}^{(1)} = 0 \ .$$

For $\mu = 2$ the phase factor in Eq. (A10) is unity so only the trivial result ${}^{2}h_{14}^{(1)} = {}^{2}h_{14}^{(1)}$ is obtained. The next useful result comes from the third neighbors whose geometry is shown in Fig. 8. Taking the C_2 axis as the perpendicular bisector of $\vec{\rho}_{14}$ in Fig. 1, and $\vec{r}_3$ the vector between third neighbors to be in a plane perpendicular to this C_2 axis, then

$$\begin{aligned} &C_2|\mu R_{m1}\rangle = |\mu R_{m'4}\rangle \ , \quad C_2|\mu R_{m4}\rangle = |\mu R_{m'1}\rangle \ , \\ &C_2|\mu R_{m2}\rangle = |\mu R_{m'3}\rangle \ , \quad C_2|\mu R_{m3}\rangle = |\mu R_{m'2}\rangle \ . \end{aligned} \tag{A11}$$

This together with Eq. (A1) gives

$${}^{\mu}h_{41}^{(3)}(\vec{r}_3) = {}^{\mu}h_{14}^{(3)}(-\vec{r}_3) \ ,$$

$$ {}^{\mu}h_{23}^{(3)}(\vec{r}_3) = {}^{\mu}h_{32}(-\vec{r}_3) \ . \tag{A12} $$

The Hermitian nature of $\mathcal{H}$ implies

$$ {}^{\mu}h_{41}^{(3)}(\vec{r}_3) = [{}^{\mu}h_{14}^{(3)}(-\vec{r}_3)]^* \ , $$
$$ {}^{\mu}h_{23}^{(3)}(\vec{r}_3) = [{}^{\mu}h_{32}^{(3)}(-\vec{r}_3)]^* \ . \tag{A13} $$

Equations (A12) and (A13) together show that ${}^{\mu}h_{23}^{(3)}(\vec{r}_3)$ and ${}^{\mu}h_{14}^{(3)}(\vec{r}_3)$ are real. This is true for both $\mu = 1$ and $\mu = 2$. The transformation properties of the $|\vec{R}_{mi}\rangle$ under the other two C_2 operations of D_3^7, i.e., C_2' and C_2'', involve phase factors because $C_2' = C_3 C_2$ and $C_2'' = C_3^{-1} C_2$, and no new results are obtained from them. Once a particular operation has been physically located (e.g., C_2 in Fig. 8) it must be used consistently in analyzing the symmetry properties and phase relationships of the $h_{ij}^{l}(\vec{r}_l)$ for all l. Phase relationships between the individual $h_{ij}^{(l)}$ for ion pairs of a given type are required in order to factorize out a particular $h_{ij}^{(l)}(\vec{r}_l)$ in the exciton dispersion expressions. We illustrate this by the third-neighbor TOE. For $\mu = 1$, the $|R_{mi}\rangle$ transform in the C_3 site group like a_3, a_2, a_3, a_2 for $i = 1, 2, 3, 4$, respectively. Using this in Eq. (A1) and referring to Fig. 8 we get

$$ {}^{1}h_{41}^{(3)}(\vec{r}_3) = e^{2i\pi/3}\,{}^{1}h_{41}(C_3\vec{r}_3) = e^{-2i\pi/3}\,{}^{1}h_{41}(C_3^{-1}\vec{r}_3) $$
and (A14)
$$ {}^{1}h_{23}^{(3)}(\vec{r}_3) = e^{2i\pi/3}\,{}^{1}h_{23}(C_3\vec{r}_3) = e^{-2i\pi/3}\,{}^{1}h_{23}(C_3^{-1}\vec{r}_3) \ . $$

†The Lincoln Laboratory portion of this work was sponsored by the Department of the Air Force.

[1]J. Frenkel, Phys. Rev. 37, 17 (1931). Specific references to the exciton description of the excited states of transition-metal insulators were made by G. W. Pratt and R. Coelho, *ibid.* 116, 281 (1959); A. M. Clogston, J. Appl. Phys. 31, 1985 (1960).

[2]V. V. Eremenko and A. I. Belyaeva, Fiz. Tverd. Tela 5, 2877 (1963) [Sov. Phys. Solid State 5, 2106 (1964)].

[3]J. P. van der Ziel, Phys. Rev. Letters 18, 237 (1967).

[4]J. W. Allen, R. M. Macfarlane, and R. L. White, Phys. Rev. 179, 523 (1969).

[5]K. Aoyagi, K. Tsushima, and S. Sugano, Solid State Commun. 7, 229 (1969).

[6]R. S. Meltzer, Phys. Rev. B 2, 2398 (1970).

[7]S. Freeman and J. J. Hopfield, Phys. Rev. Letters 21, 910 (1968); R. S. Meltzer, M. Y. Chen, D. S. McClure, and M. Lowe-Pariseau, *ibid.* 21, 913 (1968).

[8]S. Sugano and I. Tsujikawa, J. Phys. Soc. Japan 13, 899 (1958); S. Sugano and Y. Tanabe, *ibid.* 13, 880 (1958); S. Sugano and M. Peter, Phys. Rev. 122, 381 (1961); R. M. Macfarlane, J. Chem. Phys. 39, 3118 (1963).

[9]R. M. Macfarlane, J. W. Allen, and S. Sugano, Bull. Am. Phys. Soc. 15, 338 (1970).

[10]G. Dresselhaus, J. Phys. Chem. Solids 1, 14 (1956).

[11]Y. Onodera and Y. Toyozawa, J. Phys. Soc. Japan 22, 833 (1967).

[12]R. S. Knox, J. Phys. Chem. Solids 9, 238 (1959).

[13]A. S. Davydov and E. F. Sheka, Phys. Status Solidi 11, 877 (1965).

[14]J. Jortner, S. A. Rice, J. L. Katz, and S. Choi, J. Chem. Phys. 42, 309 (1965).

[15]D. P. Craig and P. C. Hobbins, J. Chem. Soc. 539 (1955).

[16]D. P. Craig and S. H. Walmsley, *Physics and Chemistry of the Organic Solid State* (Interscience, New York, 1963), Vol. 1, p. 586.

[17]A. R. Lacey and L. E. Lyons, J. Chem. Soc. 5393 (1964). This is the Davydov splitting measured in the zero-phonon line.

[18]D. S. McClure, in *Solid State Physics*, edited by F. Seitz and D. Turnbull (Academic, New York, 1959), Vol. 8, p. 1.

[19]S. D. Colson, D. M. Hanson, R. Kopelman, and G. W. Robinson, J. Chem. Phys. 48, 2215 (1968).

[20]D. M. Hanson, R. Kopelman, and G. W. Robinson, J. Chem. Phys. 51, 212 (1969).

[21]D. M. Hanson and G. W. Robinson, J. Chem. Phys. 43, 4174 (1965).

[22]R. H. Clarke and R. M. Hochstrasser, J. Chem. Phys. 46, 4532 (1967).

[23]R. E. Newnham and Y. M. de Haan, Z. Krist. 117, 235 (1962).

[24]B. N. Brockhouse, J. Chem. Phys. 21, 961 (1953).

[25]G. F. Koster, in *Solid State Physics*, edited by F. Seitz and D. Turnbull (Academic, New York, 1957), Vol. 5, p. 173.

[26]J. C. Slater, *Quantum Theory of Molecules and Solids* (McGraw-Hill, New York, 1965), Vol. 2, p. 417.

[27]P. W. Anderson, Phys. Rev. 115, 2 (1959).

[28]This is in contrast to the magnon case where the subspace of interest includes states with two, and more, ions excited.

[29]E. J. Samuelsen, Physica 43, 353 (1969). In the magnon case h_{12} and h_{43} are not TOE matrix elements, but off-diagonal elements between the ground state and states with two ions excited.

[30]Y. Tanabe, T. Moriya, and S. Sugano, Phys. Rev. Letters 15, 1023 (1965).

[31]This is an extension of the two-sublattice treatment of exciton-magnon absorption by Sell, Greene, and White, Phys. Rev. 158, 489 (1967).

[32]The two-site functions for nearest-neighbor pairs (there are N such sets in the crystal), i.e., $|\vec{R}_{ni}, \vec{\rho}_{14}^{0}\rangle$, induce the $\vec{k} = 0$ representations $2E$ of D_3^7.

[33]R. A. Alikhanov, Z. Dimitrijević, A. Kowalska, S. Kraśnicki, H. Rzany, J. Todorović, and A. Wanic, Phys. Status Solidi 32, 41 (1969).

[34]E. J. Samuelsen, M. T. Hutchings, and G. Shirane, Solid State Commun. 7, 1043 (1969); Physica 48, 13 (1970).

[35]J. W. Allen, Bull. Am. Phys. Soc. 16, 379 (1971).

[36]R. E. Dietz and A. Misetich, in *Proceedings of the Conference on Localized Excitations in Solids, Irvine, California*, 1967 (Plenum, New York, 1968), p. 366.